

Crystallization of Transmembrane Proteins *in cubo*: Mechanisms of Crystal Growth and Defect Formation

Yasser Qutub¹, Ilya Reviakine¹, Carrie Maxwell², Javier Navarro²
Ehud M. Landau^{2*} and Peter G. Vekilov^{1*}

¹Department of Chemical Engineering, University of Houston, Houston, TX 77204 USA

²Membrane Protein Laboratory Department of Neuroscience and Cell Biology, University of Texas-Medical Branch Galveston, TX 77555, USA

Crystallization of membrane proteins is a major stumbling block en route to elucidating their structure and understanding their function. The novel concept of membrane protein crystallization from lipidic cubic phases, “*in cubo*”, has yielded well-ordered crystals and high-resolution structures of several membrane proteins, yet progress has been slow due to the lack of understanding of the molecular mechanisms of protein transport, crystal nucleation, growth, and defect formation *in cubo*. Here, we examine at molecular and mesoscopic resolution with atomic force microscopy the morphology of *in cubo* grown bacteriorhodopsin crystals in inert buffers and during etching by detergent. The results reveal that crystal nucleation occurs following local rearrangement of the highly curved lipidic cubic phase into a lamellar structure, which is akin to that of the native membrane. Crystals grow within the bulk cubic phase surrounded by such lamellar structures, whereby transport towards a growing crystalline layer is constrained to within an individual lamella. This mechanism leads to lack of dislocations, generation of new crystalline layers at numerous locations, and to voids and block boundaries. The characteristic macroscopic lengthscale of these defects suggests that the crystals grow by attachment of single molecules to the nuclei. These insights into the mechanisms of nucleation, growth and transport *in cubo* provide guidance en route to a rational design of membrane protein crystallization, and promise to further advance the field.

© 2004 Elsevier Ltd. All rights reserved.

Keywords: transmembrane proteins; lipidic cubic phases; molecular-resolution AFM; crystallization mechanisms; nucleation

*Corresponding authors

Introduction

Genomic sequencing has revealed that about one-third of the human genome codes for proteins having at least one transmembrane segment,¹ yet, whereas the protein data bank comprises more than 27,000 entries, fewer than 60 represent distinct membrane protein structures†. While several of these were obtained by electron crystallography using two-dimensional crystals or other low-dimensional arrays,^{2–8} the majority of the structures are solved by X-ray diffraction from three-dimensional crystals.^{9–14} Preparation of diffraction-quality

crystals remains the major bottleneck in the pursuit of high-resolution structures of membrane proteins.¹⁵ Therefore, improvements of the existing, detergent micelle-based crystallization methods,¹² as well as entirely new approaches are sought continuously.^{10,16–19} The concept of crystallizing membrane proteins in lipidic cubic phases (*in cubo*)²⁰ is a recent addition to the arsenal of crystallization methods available to crystallographers. Since its introduction, this method has yielded well-ordered crystals and X-ray structures of several membrane proteins.²¹ While the mechanisms of crystallization of soluble proteins have been studied in considerable detail,^{22–24} and it has been argued that the crystallization of detergent-solubilized membrane proteins may follow similar mechanisms,¹² a hypothetical mechanism for the *in cubo* crystallization of transmembrane proteins has been proposed only recently,²⁵ and a comprehensive general understanding of the

Abbreviations used: AFM, atomic force microscopy; bR, bacteriorhodopsin; OG, β -octylglucoside.

E-mail addresses of the corresponding authors: vekilov@uh.edu; emlandau@utmb.edu

† <http://www.rcsb.org/pdb>

mechanisms involved in such crystallization is still missing.

Due to the structure of the lipidic cubic phase,²⁵ growth conditions *in cubo* differ in essential ways from those in solution. Indeed, in the lipidic matrix, an integral membrane protein is confined to the three-dimensional network of the curved bilayers, and protein transport occurs along this network. On the other hand, the transport of small molecules involved in crystallization (buffers, precipitants, additives, etc.) is confined to the complementary three-dimensional network of aqueous channels that interpenetrates the lipid network.²⁶ The transport conditions may be complicated even further in the vicinity of a crystal, where the lipid phase is assumed to convert from a three-dimensional network into a stack of lamellar layers.²⁵ In contrast, during solution crystallization of both soluble proteins and detergent-solubilized membrane proteins, the building blocks of the crystals, the protein molecules, and the small-molecule precipitants and additives are transported through the same unrestricted isotropic three-dimensional space. Crystals of soluble proteins grow from solution by the attachment of molecules to new crystalline layers spreading on the crystal's surfaces. These layers are generated either on screw dislocations,^{27–32} two-dimensional nuclei,^{29,31,33–36} or three-dimensional nuclei.^{37,38} The errors in these mechanisms that lead to defects have been catalogued, so that the defect-generation sequences are understood at a reasonable level.^{23,35,39–41} However, because of the entirely different and more complex nature of transport towards the growing crystal during crystallization *in cubo*, it is likely that the implementations of these mechanisms of crystallization and defect formation are modified significantly.

Atomic force microscopy (AFM)⁴² has become an important tool in the investigations of biological systems.^{43–53} AFM has produced a plethora of novel insights into the crystallization processes of soluble proteins at the macroscopic, mesoscopic and molecular levels;^{35,46,48–51} however, success with 3-D crystals of membrane proteins has been limited.^{52,53}

Here, we employ AFM to study the morphology of bacteriorhodopsin (bR) crystals grown from a lipidic cubic phase. We address the following issues, essential for the understanding of the mechanisms of crystal growth *in cubo*: How does the structure of the cubic phase influence the transport of proteins and small molecules? How are the transport conditions modified by the defects in the lipid bilayer network? Do the crystals grow by spreading of layers and, if so, what are the mechanisms of generation of these layers? Are the typical types of crystalline defects, point (vacancies and misplaced molecules), linear (dislocations), planar (stacking faults, block boundaries), and three-dimensional (voids and occlusions), present in lipidic cubic phase grown crystals? How is defect formation influenced by the conditions of growth?

Results

Morphology and packing of bR crystals

Hexagonal bacteriorhodopsin crystals (Figure 1) were grown in the lipidic cubic phase (60–70% (w/w) monoolein) according to the published procedure.²⁰ Crystals belong to space group $P6_3$, with unit cell dimensions $a=b=62$ Å, $c=108$ Å, $\gamma=120^\circ$.²⁰ Molecules pack in a polar lamellar structure, with planar hexagonal arrays of the protein trimers stacked on top of each other, related by a 6-fold screw axis along the c -direction. The packing arrangement of the protein within each layer is identical to that found in native purple membranes, where bacteriorhodopsin trimers are arranged in a hexagonal lattice with $a=62(\pm 2)$ Å.³

Typical images of the hexagonal face of bR crystals in 1.8 M Sørensen buffer (see Materials and Methods) are shown in Figure 2. The lower-magnification image in Figure 2(a) reveals that the face consists of co-planar blocks of approximately 700 nm by 900 nm, separated by channels. The surface roughness, seen in Figure 2(a) and addressed further below, was limited to the mesoscopic lengthscale; on the molecular level, the surface was relatively smooth and the crystal lattice was clearly visible using a higher magnification (see Figure 2(b)). The lattice constants, determined from the Fourier transform (see the inset in Figure 2(b)), $a=86(\pm 4)$ Å, $b=89(\pm 5)$ Å, $\gamma=126^\circ$ are larger than those determined by X-ray crystallography, most likely due to distortions

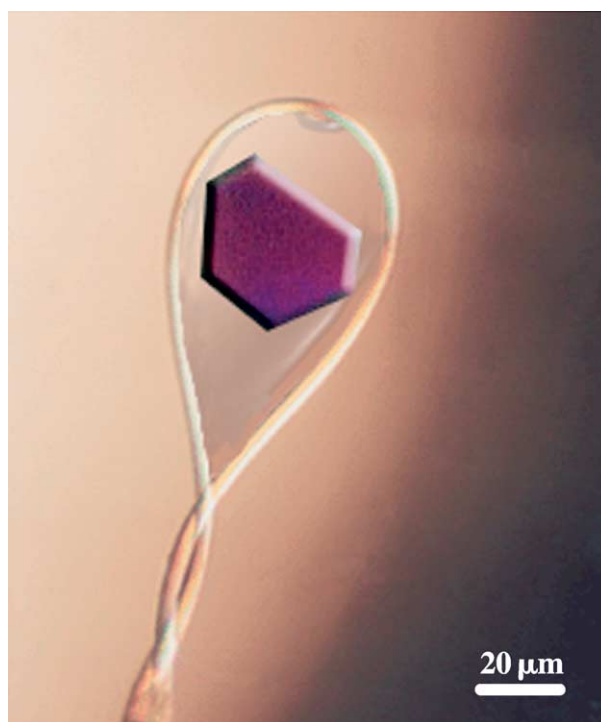


Figure 1. An optical microscopy image of a hexagonal bR crystal grown in monoolein cubic phase. The crystal was harvested using Cryoloop[®], as shown in the image.

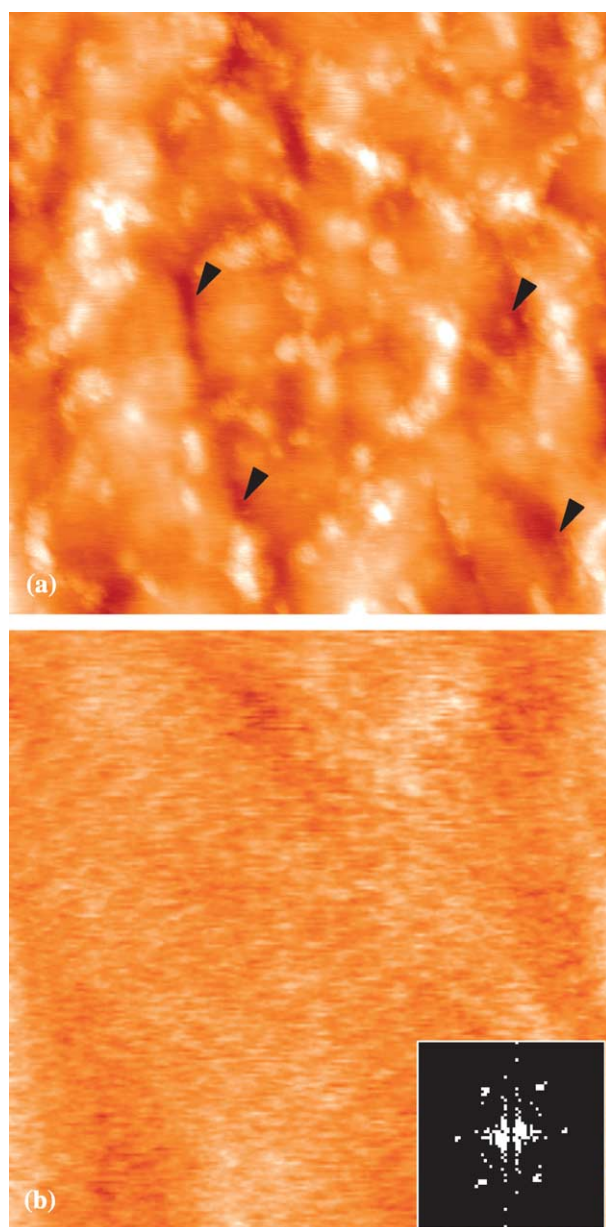


Figure 2. AFM images of the hexagonal face of a 3-D bR crystal, such as the one shown in Figure 1. (a) A tapping mode AFM image (frame size $1.37\ \mu\text{m}$, Z-scale $50\ \text{nm}$) of the surface of the bR crystal. The topography reveals the rough nature of the surface of 3-D bR crystals. The surface consists of co-planar blocks ($700 \times 900\ \text{nm}^2$) separated by channels. The black arrowheads point to the channels dividing the blocks. (b) A tapping mode AFM image (frame size $158\ \text{nm}$, Z-scale $10\ \text{nm}$) of a region from (a). The image reveals a hexagonal lattice with parameters $a = 86(\pm 4)\ \text{\AA}$, $b = 89(\pm 5)\ \text{\AA}$, $\gamma = 126^\circ$. Inset: A Fourier transform of the image in (b).

caused by the use of an O-ring during imaging,^{54,55} which was required to prevent evaporation of the buffer.

In agreement with the X-ray data, the crystals were found to consist of stacks of lamellae (see Figure 3). The thickness of the individual lamellae

was determined from over 50 images and the statistical distribution of the data is shown in Figure 4. Thickness values of 11 nm, 21 nm, and 31 nm represented by the peaks of the histograms in Figure 4. These thicknesses correspond approximately to one, two, and three lattice parameters, respectively, in the *c*-direction, $c = 108\ \text{\AA}$.²⁰ Lamella thickness of $\sim 5\text{--}6\ \text{nm}$, which corresponds to $0.5c$, or the thickness of one purple membrane sheet,⁵⁶ is indicated with a red arrowhead in Figure 4(c). Thus, the overall organization of the $P6_3$ bR crystals grown in the lipidic cubic phase as observed by AFM is consistent with that derived from X-ray crystallographic analysis.

The overall appearance of the large hexagonal (001) face of bR crystals is quite unusual. In contrast to the molecularly smooth terraces separated by unimolecular steps that are observed typically on surfaces of crystals of soluble proteins,^{32,35,46,48–50} the stacks of crystalline layers (e.g. see Figure 3), have various heights and sizes. As a result, the crystal face exhibits an uneven morphology, illustrated in Figure 2(a). The lamellae appear to have random shapes and are remarkably rough at the edges (Figure 3(b)), another stark contrast to what is observed commonly with soluble proteins. Between the stacks of lamellae, gaps that penetrate to depths $> 1\ \mu\text{m}$ into the crystal face are seen. In comparison, stacks of straight, uniform edges of the lamellae were observed at the intersection of the hexagonal and prismatic faces (see Figure 3(e)).

Etching of bR crystals

To further characterize the defect structure of bR crystals grown *in cubo*, we monitored their dissolution *in situ*. For this, bR crystals were exposed to a 3 mg/ml solution of β -octylglucoside (OG) in 1.8 M Sørensen buffer. A time-lapse series of images recorded at intervals of approximately two minutes shortly after the crystal was exposed to the solution of OG is shown in Figure 5. The lamella edges retreat at approximately similar rates. On some of the lamellae, it was possible to observe rows spaced $\sim 5.4\ \text{nm}$ apart (Figure 5(h)). The spacing, determined from the Fourier transform in the inset in Figure 5(i), is comparable to the lattice constant $a = 6.2\ \text{nm}$.²⁰ On the basis of this observation, we conclude that these are molecular rows of bR trimers.

The characteristic roughness of the features in Figure 5(a)–(g) is similar to that in Figure 3 and, importantly, is preserved during the dissolution process.

Comparing the locations of the layers in Figure 5(a)–(g), we estimate the velocity of step retraction as $3(\pm 1)\ \text{nm/s}$. These rates are comparable to the rates of step propagation during growth and dissolution of soluble proteins.^{32,57}

The etching experiments offer further support to the correspondence of the surface morphology of the mature crystal, as observed with the AFM, to the morphology of a growing crystal. Indeed, the

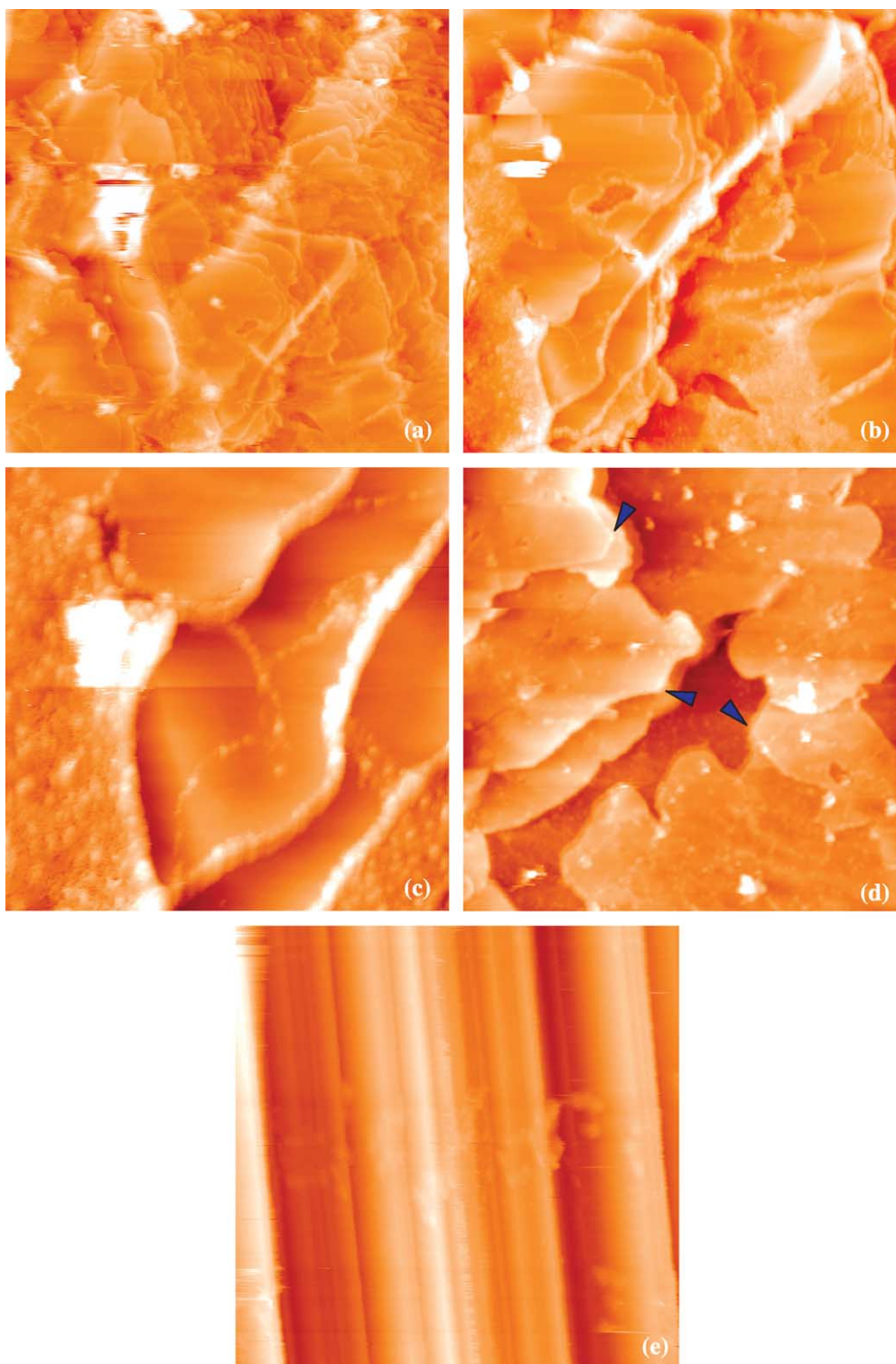


Figure 3. Structure of bR crystals revealed by AFM. (a), (b) and (c) Tapping mode AFM images of a bR crystal in 1.8 M Sørensen buffer (pH 5.6) showing stacks of lamellae. Frame sizes: (a) 10 μm , (b) 5 μm , and (c) 1.6 μm . (d) A tapping mode image (frame size 5.4 μm) of a different bR crystal in 1.8 M Sørensen buffer (pH 5.6) showing stacks of lamellae. Facets with characteristic $\sim 120^\circ$ angles are observed (indicated by arrowheads). (e) A contact mode image (frame size 5 μm) of the tapered region at the intersection of the hexagonal face with the prismatic face. The image was acquired in 25 mM Sørensen solution (pH 5.6). Z-scales: (a) 900 nm, (b) 350 nm, (c) 200 nm, (d) 300 nm, and (e) 1200 nm.

detergent treatment illustrated by [Figure 5](#) leads to a rather orderly dissolution of the crystal that could not have produced any of the features observed prior to the treatment. This is not surprising: lipase,

used to digest the lipid phase for the purpose of extracting the crystals from the lipidic matrix prior to AFM examination, does not hydrolyze the purple membrane lipids present within the crystals. Thus,

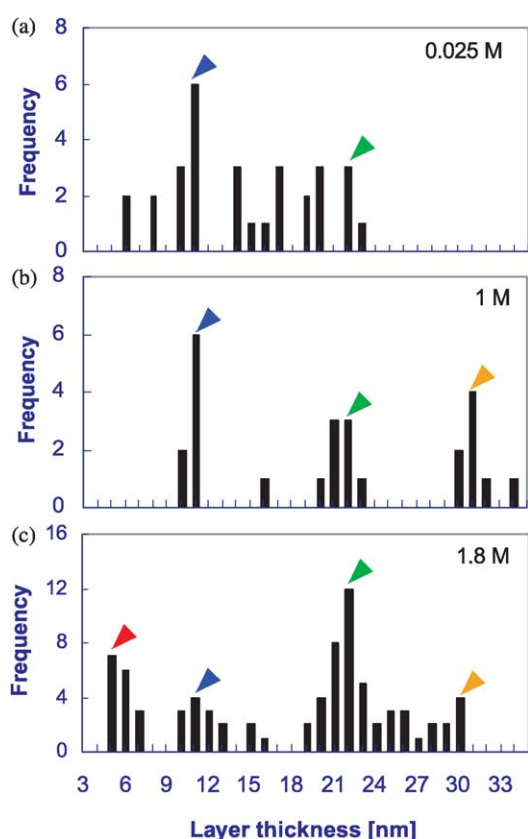


Figure 4. Distribution of the thickness of crystal layers determined from more than 50 images from six crystals. The concentrations of Sørensen buffer at which the bR crystals were imaged are shown in the plots. Red, blue, green, and orange arrowheads indicate the peaks that correspond to thickness of approximately 5, 11, 21, and 31 nm, respectively.

hydrolysis of the cubic phase matrix likely leaves the crystal largely intact.

Nucleation of salt crystals on the surface of bR crystals

Angular objects with a characteristic angle of 72° between the edges were observed on the hexagonal (001) face of bR crystals held at a high concentration (1.8 M) of Sørensen buffer (Figure 6). This angle is characteristic of potassium dihydrogen phosphate (KH_2PO_4).⁵⁸ We assume that these triangular structures are small crystals of KH_2PO_4 that have nucleated on the surface of the bR crystal. To test this assumption, bR crystals with such structures were kept for two days in a solution containing a lower concentration (0.5 M) of Sørensen buffer, and then imaged. The triangular structures were no longer present. bR crystals are grown from saturated solutions of the phosphate salts and the nucleation and growth of the phosphate crystals⁵⁸ is faster by orders of magnitude than those of bR. Since the solubility of the phosphates is strongly dependent on temperature,⁵⁹ minor temperature

instabilities can lead to supersaturated phosphate solutions and formation of the phosphate crystals. These phenomena could take place as bR crystals grow in the lipidic cubic phase in the presence of high concentrations of Sørensen salt, and can result in the incorporation of salt crystals in the bulk of the bR crystal. This would stress the bR material severely, and the strain may in turn be resolved by the formation of other two-dimensional and three-dimensional defects.^{60,61} Thus, the incorporation of KH_2PO_4 crystals would ultimately lead to poor diffraction quality of some of the bR crystals.

Defects

Besides the block boundaries, discussed above, the defects detected on the (001) face of the bR crystals include irregularly shaped holes (Figure 7(a)) and cracks (Figure 7(c)–(e)).

Exposing crystals to various concentrations of salt revealed the elastic character of the lamellae: in response to the osmotic stress imposed by immersing the crystal grown in a solution of 1.8 M Sørensen salt into a solution of 25 mM Sørensen salt, the surface wrinkled, but did not fracture (Figure 7(b), (e) and (f)). We attribute the wrinkling to separation between adjacent lamellae in the regions where the interactions between them is weak, likely due to voids or other defects.

Discussion

The mechanisms of crystallization *in cubo*

A molecular mechanism for crystallization *in cubo*, based on polarization microscopy and low-angle X-ray diffraction studies, was put forth by Nollert *et al.*²⁵ The basic premise of that model is that protein crystallization *in cubo* is initiated by dehydration of the protein-containing lipidic cubic phase, which triggers a decrease in unit cell size, an increase of membrane curvature, and a hydrophobic mismatch between the membrane protein and the curved lipid bilayers. Dehydration is induced by the added salt. It was speculated that crystallization is accompanied by a cubic-to-lamellar transformation in lipid structure, and that this transformation is facilitated by the protein,²⁵ probably due to the increased stiffness of the protein-lipid layers relative to their protein-free counterparts.

The main elements of this mechanism²⁵ triggered by the salt-induced curvature increase can be classified as follows: (i) fluctuation of concentration leads to a locally high concentration of bR at random locations in the lipidic cubic phase; (ii) the high concentration of protein triggers a local transformation of the cubic phase into a lamellar structure; (iii) crystal nucleation occurs in the lamellar region; (iv) the growth of the crystal is fed from the bulk cubic phase *via* a several micrometer-wide lamellar region, which is

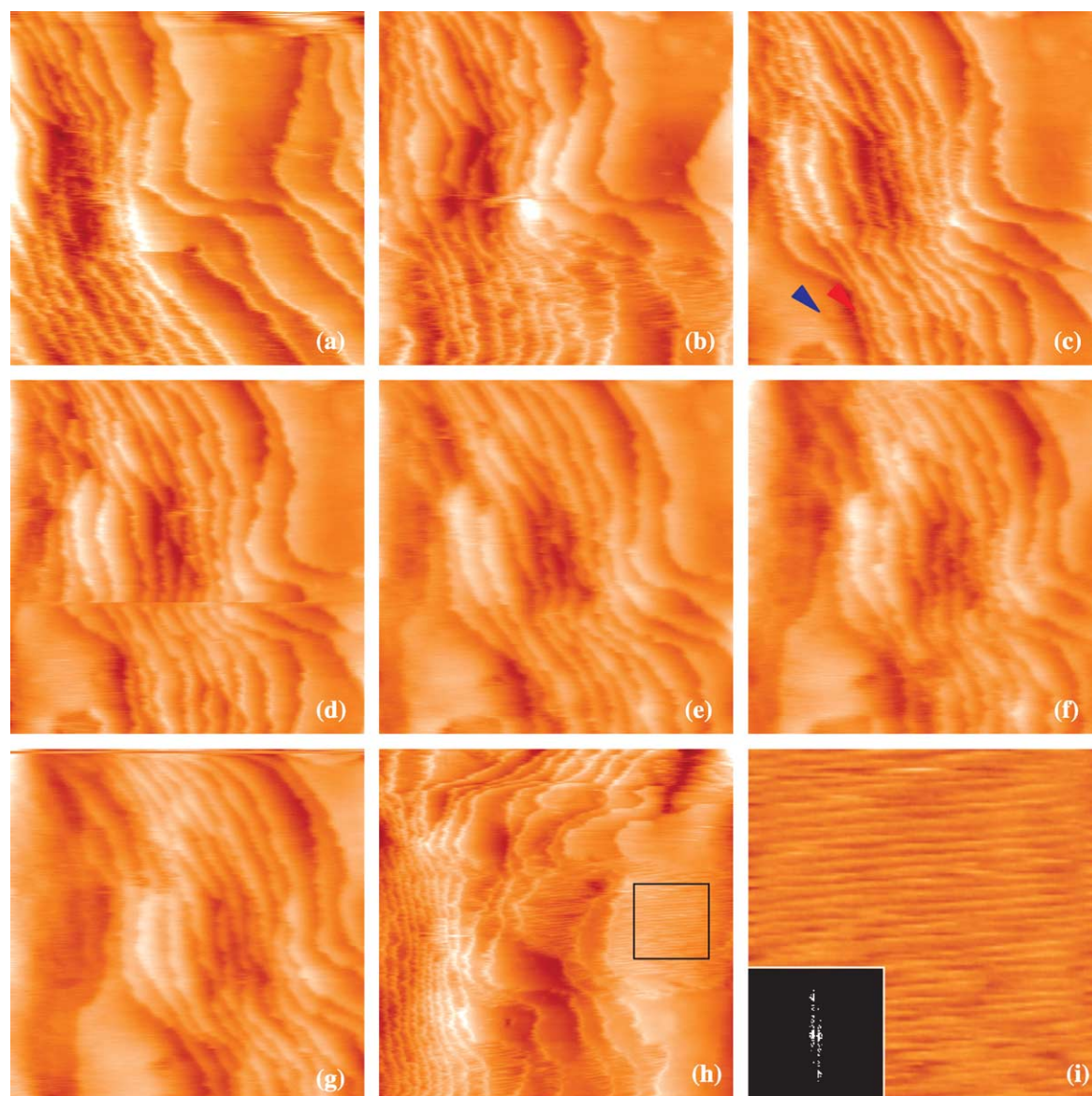


Figure 5. Etching of bR crystal observed by addition of octyl glucoside. (a)–(g) A time-lapse series of $403 \times 403 \text{ nm}^2$ (Z-scale: 50 nm) contact mode images of the hexagonal face of a bR crystal acquired shortly after exposure to 1.8 M Sørensen buffer containing 3 mg/ml of OG. The images were recorded consecutively, each at an acquisition time of two minutes. Edges of lamellae, visible in these images, are changing shape and retracting. The distances between a defect (blue arrowhead) and an edge of a lamella (red arrowhead) was found to increase from 34 nm in (c) to 48 nm in (e). (h) A contact mode image (frame size 627 nm) revealing molecular rows indicated with the black rectangle. (i) A magnification (frame size 160 nm) of the area is indicated with the black rectangle in (h). The image reveals rows separated by $\sim 5.4 \text{ nm}$ determined by the Fourier transform shown in the inset. Z-scale: (h) 70 nm and (i) 30 nm.

preserved around the crystal as its dimensions increase.

An alternative to the sequence of steps (i)–(ii) would be a mechanism whereby random appearances of lamellar regions within the dehydrated lipidic phase (which can be viewed as fluctuations of the structure of the lipidic phase) lead to a local increase in protein concentration and crystal nucleation. While there is no experimental evidence to distinguish the (i)–(ii) and (ii)–(i) scenarios, this question may have significant practical consequences. For instance, the (ii)–(i) scenario implies that numerous cubic phase structure fluctuations

occur and are not “filled” by a nucleation event, so efforts should be applied towards enhancing the nucleation of the crystals within existing lamellar regions. If the (i)–(ii) scenario operates, one should try to enhance the protein density fluctuations in the lipidic cubic phase, for instance by increasing the attraction between the protein molecules suspended in it. Since the primary fluctuations lead to either isotropic or anisotropic objects, the issue could be resolved by experiments with scattering of polarized radiation.

Prior to this work, element (iv) of the above mechanism has been supported by just one piece of

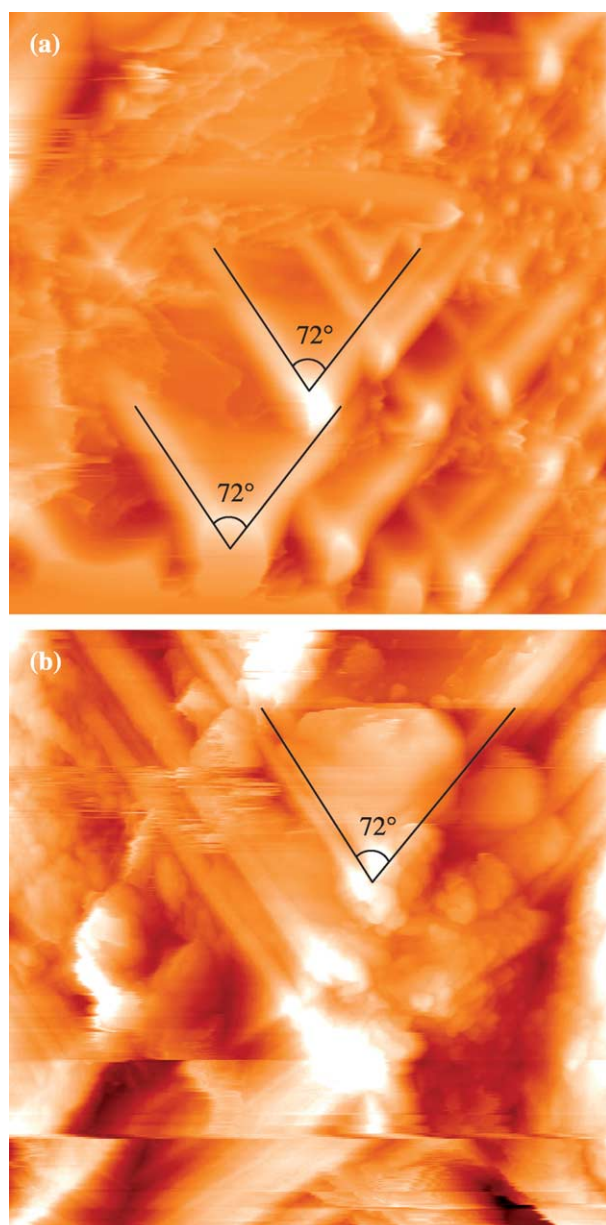


Figure 6. Phosphate salt crystals observed on the surface of bR crystals. The edges of the phosphate crystals meet at a characteristic angle of 72° , indicated by the black lines. (a) A contact mode AFM image (frame size $6.34\ \mu\text{m}$) and (b) a tapping mode AFM image (frame size $2.86\ \mu\text{m}$) of the surface of bR crystals in saturated $1.8\ \text{M}$ Sørensen buffer.

evidence: the finding that bR crystals within the bulk cubic phase are surrounded by a halo of bi-refractive material.²⁵ In further support, we note that the surface of bR crystals is exceedingly rough, comprised of stacks of unfinished crystalline layers that are non-contiguous, of arbitrary shapes and sizes, and characterized by excessive edge roughness. This likely is a consequence of transport towards individual layers *via* the lamellar phase surrounding the crystal so that transport of protein within each layer is essentially independent of that

in other layers. Thus, the mesoscopic and macroscopic processes of nucleation and growth in each layer are independent of those occurring in other layers. The only coordination between layers occurs at the molecular lengthscale, within the crystal lattice, ensuring that every new layer is aligned with the underlying layers. This is similar to what is observed in soluble proteins, for which growth *via* layers in registry with underlying layers is one of the two major growth modes.^{29,31,33–36} However, with soluble proteins, coordination between successive layers occurs also on the macroscopic lengthscale as a result of the overlap of the supply fields of the individual steps.

According to this model, each growing embryo of a crystalline layer is fed by protein molecules only from within the lamellar layer to which this embryo belongs. If several co-planar nucleation events occur, the regions between them will become depleted of protein. The outward growth of these sources will be faster than the inward growth, and inner regions of the crystal face will contain areas that may never be filled with crystalline material. During our observations, the lipid phase filling the non-crystalline voids is digested by the lipase and appears as gaps in the crystal (Figure 3). In agreement with this explanation, in Figure 3 the edges of crystalline layers facing other crystalline layers within the same lamellar layers are rough. This suggests cessation of growth due to exhaustion of the material. Such growth cessation is the likely reason for the presence in Figure 3 and of $\sim 5\text{--}6\ \text{nm}$ thick layers, a high free-energy configuration, corresponding to half of the thickness of one purple membrane sheet.⁵⁶ The edges of the crystalline layers that are open for supply of building blocks within the same lamellar layer as seen in Figure 3(d) are faceted, likely because their growth stopped in a slowly decreasing concentration environment as equilibrium between the crystal and the cubic phase was approached.

This mechanism suggests that edges of the crystalline layers at the crystal's facets, which are well supplied with protein, will be oriented along crystallographic directions, as in the case of crystals of soluble proteins. Accordingly, the overall shape of the crystal in Figure 1 is faceted. Furthermore, at the intersection between the prismatic and the hexagonal faces of bR crystals, shown in Figure 3(e), the crystalline layers have straight edges, likely along a crystallographic direction.

Another consequence of the two-dimensional mode of transport is the possibility of new crystals nucleating in the immediate vicinity of a growing crystal. Such a process is unlikely with isotropic three-dimensional transport, where a growing crystal depletes the solution around it, but is possible if crystallization in one lamella does not compete for supply with growth in neighboring lamellae. An example is presented in Figure 8, where a small crystal incorporated into the larger crystal at an inclination of about $<5^\circ$ with respect to the crystal face is visible. Judging from the size of

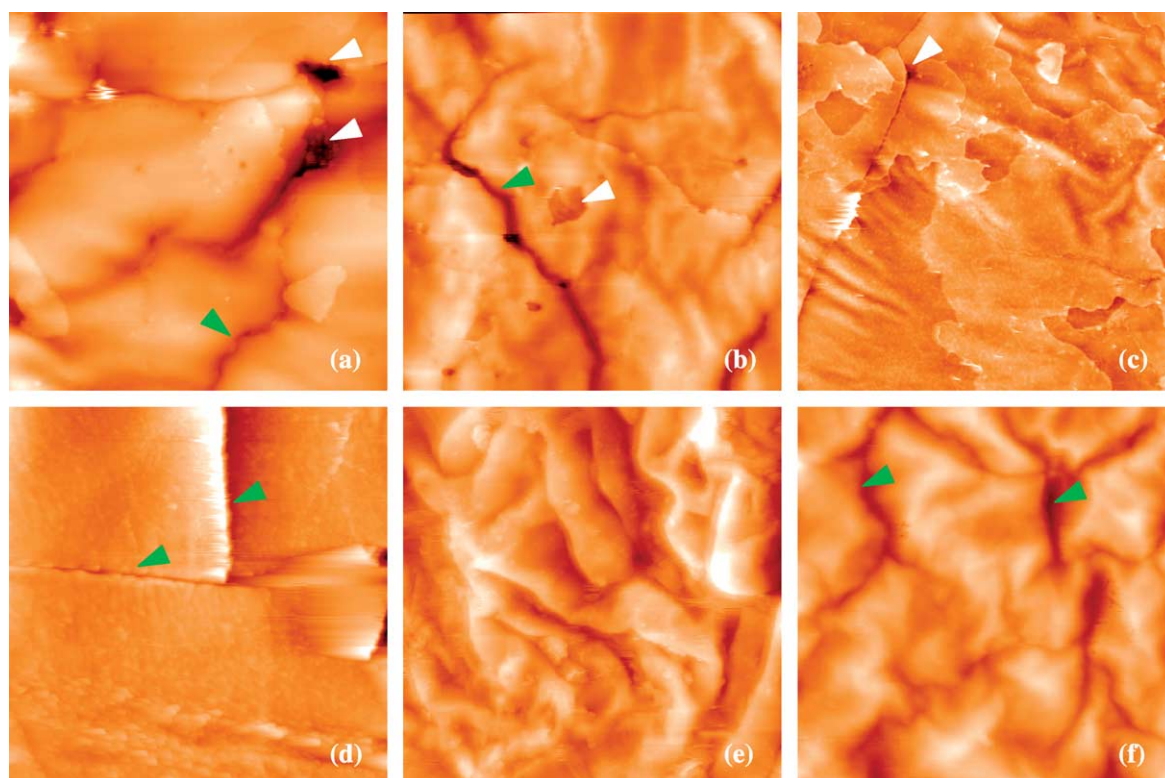


Figure 7. Block boundaries, holes, and cracks observed on the surface of bR crystals. White arrowheads point to holes in the surface; green arrowheads point to cracks. (a) A tapping mode AFM image (frame size 5 μm , Z-scale 500 nm) and (b) a contact mode AFM image (frame size 8.81 μm , Z-scale: 400 nm) both in the presence of 25 mM Sørensen buffer. (c) A tapping mode AFM image (frame size 10 μm , Z-scale: 300 nm) and (d) a tapping mode AFM image (frame size 10 μm , Z-scale: 500 nm) both in 1.8 M Sørensen buffer. (e) and (f) Images revealing folding and swelling of the surface, seen along with cracks shown in (f). Image sizes: (a) 5 μm , (b) 8.81 μm , (c) 10 μm , (d) 10 μm , (e) 5.68 μm , and (f) 8.85 μm . Z-scale: (a) 500 nm, (b) 400 nm, (c) 300 nm, (d) 500 nm, (e) 1600 nm, and (f) 750 nm.

the smaller crystal, it likely nucleated as close as 1 μm away from the surface of the large one.

Lipidic phase rearrangement and crystal nucleation

The morphological features of bR crystals observed with AFM offer a strong support to element (iii) of the above mechanism, that the rearrangement of the lipid phase into a lamellar structure precedes crystal nucleation. The observation of smaller crystal nucleated within the lamellar structure surrounding a larger crystal discussed above, shows the feasibility of crystal nucleation within lamellar lipid layers. Furthermore, none of the investigated bR crystals revealed any screw dislocations, despite an extensive search for them. In crystals of soluble proteins, screw dislocations have been observed if the crystal layer parallel to the growing face is thinner than 5.5–6 nm, and not found in crystals of any protein or virus with thicker layers.³⁵ This has been explained with the quadratic dependence of the dislocation energy on its Burgers vector, equal to a whole number of layer thicknesses,⁶² so that the dislocation energy in crystals consisting of thick layers is high. If one assumes that the elastic properties of the bR crystals are similar to those of

soluble proteins,²³ one should expect screw dislocations in bR crystals whose layer thickness is ~ 5 nm (Figures 3 and 4). The lack of screw dislocations is likely due to the nucleation of the first several crystalline layers within the parallel lipid lamellar layers, so that the lamellar structure serves as a template for perfect interlayer alignment.

Attachment of molecules to growing crystals

The observations of the characteristic roughness in Figure 5 suggest that dissolution proceeds *via* the loss of single bR molecules, or of trimers from the edges of the crystalline layers to the solution. Also, dissolution is faster at the lattice defects, where the lattice strain increases the chemical potential of the molecules in the crystal and the driving force for dissolution.³² This leads to etching at the defects. In these respects, this dissolution process is similar to dissolution of crystals of soluble proteins and small molecules,⁶³ which is not surprising, because addition of detergent used in the dissolution experiments disrupts the lipidic cubic phase structure. In the case of bR crystals, the lattice defects that are preferentially etched are the boundaries between the blocks shown in Figure 2. The dense network of the block boundaries, spaced at

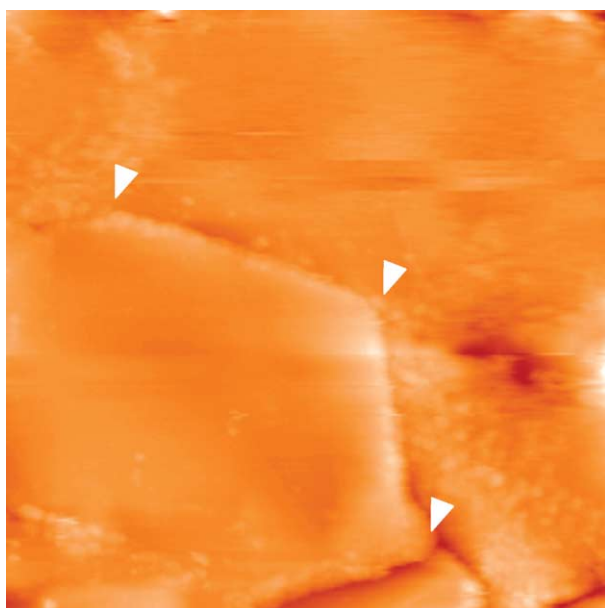


Figure 8. A small bR crystal embedded into the larger bR crystal. The small crystal is inclined with respect to the surface of the large crystal. The image was acquired in tapping mode in the presence of saturated (1.8 M) Sørensen buffer. The white arrowheads point to three of the revealed corners of the small crystal. Image size: 1.77 mm. Z-scale 250 nm.

700–900 nm apart, leads to uniform dissolution of the hexagonal face.

Another conclusion that can be drawn from the preservation of the characteristic roughness is that defects on a scale smaller than those seen in Figure 2(a), down to the molecular scale seen in Figure 5(h), are not present; they would serve as additional sources of etching and increase the roughness. The perfection of the crystalline layers at the molecular level suggests that they grew by the attachment of single molecules, rather than clusters performed in the lipidic matrix.

Despite some similarities, the dissolution of the bR crystals grown *in cubo* differs from that of soluble proteins: bR molecules released to solution are likely embedded in mixed detergent–protein micelles, and the micelle formation likely affects the dissolution kinetics. Furthermore, while in the case of soluble proteins in isotropic solution dissolution is symmetric to growth on the molecular level,⁵⁷ with deviations from the symmetry at coarser-scale phenomena, with lipidic cubic phase-grown crystals, dissolution processes have no growth equivalent at any lengthscale. Thus, during growth of the bR crystals from the lipid phase, the molecules are supplied to the crystals *via* the lipid network, while during dissolution they are released into solution. These differences affect only the rate of dissolution and do not weaken the conclusions based on observations of the layer morphology during etching.

Defect formation during *in cubo* growth

The observation that the major defects in lipidic cubic phase-grown bR crystals are of a characteristic size of a few micrometers, i.e. have the lengthscale of the transport processes, suggests that the defects are due to imperfect supply of material to the growing crystal layers. Two features of protein transport through the network of lipid bilayers merit discussion. If the rate of modified protein diffusion is significantly faster or slower than the rate of incorporation into the crystal, the non-linear coupling of the transport and growth processes may lead to kinetic instability, similar to the step bunching instability often observed with soluble proteins.³⁹ This instability results in a variable growth rate and non-uniform concentration of protein in the crystal vicinity. Such phenomena may underlie the nucleation of multiple co-planar crystalline layers, seen in Figure 3. Furthermore, the inevitable defects in the cubic and lamellar lipid phases modify the distribution of the protein in the crystal growth medium and may lead to blocked structures and other undesirable phenomena.

These considerations suggest that crystal quality may be improved by controlling the rate of transport, i.e. by selecting a lipid substance ensuring the optimal rate of membrane protein diffusion through its ordered phases. Another means of improvement may be by controlling the structure of the lipid phases so that the concentration of defects in them is minimized. For successful implementation of these pre-conditions, we need insights into the diffusion of membrane proteins through the lipid phases, as well as into the defect structure of these phases.

Materials and Methods

Crystallization of bR from lipidic cubic phases

Crystallization was conducted according to published procedure.²⁰ Purple membranes from *Halobacterium salinarum* were solubilized with β -octylglucoside (OG). Bacteriorhodopsin (bR) was purified by gel-filtration chromatography as described.⁶⁴ Purified bR was mixed with melted monoolein (MO) from NuCheck (Elysian, MN) in a glass microtube (1 mm/15 mm). The pre-crystallization mix consisted of approximately 60% (w/w) MO and 40% (w/w) bR solution. The microtubes were sealed with Parafilm and centrifuged three or four times at 10,000g for five minutes, in a temperature-controlled microcentrifuge at 20 °C, until a purple transparent gel (lipidic cubic phase) was formed at the bottom of the microtube. A Sørensen salt mixture composed of 9.48 g of KH_2PO_4 and 0.52 g of $\text{NaH}_2\text{PO}_4 \cdot \text{H}_2\text{O}$ was added to the lipidic cubic phase at a ratio of 3 : 10 (w/w) to initiate the crystallization of bR. Crystal growth was examined by optical microscopy as described.⁶⁵

Harvesting of bR crystals

The bR crystals were freed from the surrounding lipidic matrix by digesting the lipids with *Candida rugosa* lipase

(Sigma, St. Louis, MA) as described.⁶⁶ This was achieved by adding a 20 μ l aliquot of 50 mg/ml solution of the enzyme in Sørensen buffer (pH 5.6) to ~20 μ l of the preparation and leaving the mixture at room temperature overnight. The crystals that were found floating in the aqueous phase or in oleic acid droplets were harvested using a Cryolooop (Hampton Research, Aliso Viejo, CA).

Mounting of bR crystals for AFM imaging

Metal disks used as supports in the AFM experiments were coated with Teflon adhesive tape (BYTAC, Sigma, St. Louis, MO).⁶⁷ The Teflon surface was cleaned with 2% (w/v) SDS (Sigma, St. Louis, MO) and rinsed with copious amounts of de-ionized water.

bR crystals, harvested as described above, were mounted on the Teflon-coated metal discs with a two-component Epoxy glue (Cole-Parmer, Vernon Hills, IL).^{68,69} The epoxy was allowed to set for ~15 minutes, after which the samples were mounted in the atomic force microscope. The crystals were kept in Sørensen buffer (pH 5.6) throughout the procedure and never exposed to air; the buffer did not appear to interfere with the hardening of the epoxy.

Atomic-force microscopy (AFM)

The Teflon-coated metal disks supporting the adhered bR crystals in Sørensen buffer were mounted in a Nanoscope IV atomic force microscope (Veeco Metrology Group, Santa Barbara, CA), equipped with a 120 μ m ("J") scanner and a tapping mode fluid cell. In some of the experiments, an O-ring was used to prevent evaporation of solution. The fluid cell, O-ring and tubing were cleaned with 2% SDS and copious amounts of water prior to each experiment. The crystals were placed precisely under the AFM tip (oxide-sharpened silicon nitride tips, mounted on triangular cantilevers with nominal spring constants of ~0.32 N/m) with the aid of an optical microscope. The AFM was allowed to equilibrate for ~30 minutes before imaging.

Images were acquired in contact mode at constant force, or in tapping mode at constant amplitude with the cantilever excited at a drive frequency of 7.5 kHz, 8.5 kHz, or 27 kHz. Standard procedures were followed for microscope set-up.^{70,71} Scan parameters were optimized to achieve the highest image quality and to minimize tip impact. All images were acquired with crystals in Sørensen buffer. To investigate the effect of ionic strength on the crystal morphology, the ionic strength of the buffer was varied between 0.25 M and 1.8 M. All images were recorded at ambient temperature. Lamella thickness was measured using the AFM software (Veeco Metrology Group, Santa Barbara, CA).

Dissolution of bR crystals

To monitor the dissolution of bR crystals, they were exposed to 3 mg/ml of OG (Sigma, St. Louis, MO) solution in Sørensen buffer of appropriate ionic strength over periods ranging from a few minutes to several days and imaged at various time intervals.

Acknowledgements

We thank A. Oberhauser for critical comments. This work was supported by the Office of Physical

and Biological Research, NASA, through grants NAG8-1854 and NAG8-1824 to P.G.V., and Robert A. Welch Foundation grant H-1475 and NIH R01 grants GM64855, EY014218 to J.N.

References

1. Wallin, E. & von Heijne, G. (1998). Genome-wide analysis of integral membrane proteins from eubacterial, archaean, and eukaryotic organisms. *Protein Sci.* **7**, 1029–1038.
2. Henderson, R., Baldwin, J. M., Ceska, T. A., Zemlin, F., Beckmann, E. & Downing, K. H. (1990). Model for the structure of bacteriorhodopsin based on high-resolution electron cryo-microscopy. *J. Mol. Biol.* **213**, 899–929.
3. Henderson, R. & Unwin, P. N. T. (1975). Three dimensional model of purple membrane obtained by electron microscopy. *Nature*, **257**, 28–32.
4. Kühlbrandt, W., Wang, D. N. & Fujiyoshi, Y. (1994). Atomic model of plant light-harvesting complex by electron crystallography. *Nature*, **367**, 614–621.
5. Mitsuoka, K., Murata, K., Walz, T., Hirai, T., Agre, P., Heymann, J. B. *et al.* (1999). The structure of aquaporin-1 at 4.5-angstrom resolution reveals short alpha-helices in the center of the monomer. *J. Struct. Biol.* **128**, 34–43.
6. Murata, K., Mitsuoka, K., Hirai, T., Walz, T., Agre, P., Heymann, J. B. *et al.* (2000). Structural determinants of water permeation through aquaporin-1. *Nature*, **407**, 599–605.
7. Miyazawa, A., Fujiyoshi, Y., Stowell, M. & Unwin, N. (1999). Nicotinic acetylcholine receptor at 4.6 angstrom resolution: transverse tunnels in the channel wall. *J. Mol. Biol.* **288**, 765–786.
8. Stahlberg, H., Fotiadis, D., Scheuring, S., Remigy, H., Braun, T., Mitsuoka, K. *et al.* (2001). Two-dimensional crystals: a powerful approach to assess structure, function and dynamics of membrane proteins. *FEBS Letters*, **504**, 166–172.
9. Abramson, J., Smirnova, I., Kasho, V., Verner, G., Kaback, H. R. & Iwata, S. (2003). Structure and mechanism of the lactose permease of *Escherichia coli*. *Science*, **301**, 610–615.
10. Hunte, C. & Michel, H. (2002). Crystallisation of membrane proteins mediated by antibody fragments. *Curr. Opin. Struct. Biol.* **12**, 503–508.
11. Palczewski, K., Kumasaka, T., Hori, T., Behnke, C. A., Motoshima, H., Fox, B. A. *et al.* (2000). Crystal structure of rhodopsin: a G protein-coupled receptor. *Science*, **289**, 739–745.
12. Ostermeier, C. & Michel, H. (1997). Crystallization of membrane proteins. *Curr. Opin. Struct. Biol.* **7**, 697–701.
13. Pebay-Peyroula, E., Rummel, G., Rosenbusch, J. P. & Landau, E. M. (1997). X-ray structure of bacteriorhodopsin at 2.5 angstroms from microcrystals grown in lipidic cubic phases. *Science*, **277**, 1676–1681.
14. Jiang, Y. X., Lee, A., Chen, J. Y., Ruta, V., Cadene, M., Chait, B. T. & MacKinnon, R. (2003). X-ray structure of a voltage-dependent K⁺ channel. *Nature*, **423**, 33–41.
15. Abramson, J. & Iwata, S. (1999). Crystallization of membrane proteins. In *Crystallization of Proteins: Techniques, Strategies and Tips. A Laboratory Manual* (Bergfors, T., ed), pp. 199–210, International University Line, La Jolla, CA.
16. Horsefield, R., Yankovskaya, V., Tornroth, S., Luna-Chavez, C., Stambouli, E., Barber, J. *et al.* (2003). Using

- rational screening and electron microscopy to optimize the crystallization of succinate: ubiquinone oxidoreductase from *Escherichia coli*. *Acta Crystallog. sect. D*, **59**, 600–602.
17. Byrne, B., Abramson, J., Jansson, M., Holmgren, E. & Iwata, S. (2000). Fusion protein approach to improve the crystal quality of cytochrome bo(3) ubiquinol oxidase from *Escherichia coli*. *Biochim. Biophys. Acta-Bioenerg.* **1459**, 449–455.
 18. Iwata, S., Ostermeier, C., Ludwig, B. & Michel, H. (1995). Structure at 2.8-Å resolution of cytochrome c oxidase from *Paracoccus denitrificans*. *Nature*, **376**, 660–669.
 19. Faham, S. & Bowie, J. U. (2002). Bicelle crystallization: a new method for crystallizing membrane proteins yields monomeric bacteriorhodopsin structure. *J. Mol. Biol.* **316**, 1–6.
 20. Landau, E. M. & Rosenbusch, J. P. (1996). Lipidic cubic phases: a novel concept for the crystallization of membrane proteins. *Proc. Natl Acad. Sci. USA*, **93**, 14532–14535.
 21. Landau, E. M. (2003). Crystallization of membrane proteins in lipidic cubic phases. In *Methods and Results in Crystallization of Membrane Proteins* (Iwata, S., ed), pp. 39–55, International University Line, La Jolla, CA.
 22. McPherson, A. (1999). *Crystallization of Biological Macromolecules*. Cold Spring Harbor Laboratory Press, Cold Spring Harbor, NY.
 23. Vekilov, P. G. & Chernov, A. A. (2002). The physics of protein crystallization. In *Solid State Physics* (Ehrenreich, H. & Spaepen, F., eds), vol. 57, pp. 1–147, Academic Press, New York.
 24. Carter, C. W. & Sweet, R. M., eds (2003). *Macromolecular Crystallography, part C*, vol. 368, Academic Press, San Diego.
 25. Nollert, P., Qiu, H., Caffrey, M., Rosenbusch, J. P. & Landau, E. M. (2001). Molecular mechanism for the crystallization of bacteriorhodopsin in lipidic cubic phases. *FEBS Letters*, **504**, 179–186.
 26. Landau, E. M., Rummel, G., Cowan-Jacob, S. W. & Rosenbusch, J. P. (1997). Crystallization of a polar protein and small molecules from the aqueous compartments of lipidic cubic phases. *J. Phys. Chem. B*, **101**, 1935–1946.
 27. Burton, W. K., Cabrera, N. & Frank, F. C. (1951). The growth of crystals and equilibrium structure of their surfaces. *Philos. Trans. Roy. Soc. ser. A*, **243**, 299–360.
 28. Vekilov, P. G. (1993). Elementary processes of protein crystal growth. In *Studies and Concepts in Crystal Growth* (Komatsu, H., ed), pp. 25–49, Pergamon, Oxford.
 29. Vekilov, P. G. & Rosenberger, F. (1996). Dependence of lysozyme growth kinetics on step sources and impurities. *J. Crystal Growth*, **158**, 540–551.
 30. Land, T. A., DeYoreo, J. J. & Lee, J. D. (1997). An *in-situ* AFM investigation of canavalin crystallization kinetics. *Surf. Sci.* **384**, 136–155.
 31. Malkin, A. J., Kuznetsov, Y. G., Land, T. A., DeYoreo, J. J. & McPherson, A. (1996). Mechanisms of growth of protein and virus crystals. *Nature Struct. Biol.* **2**, 956–959.
 32. Reviakine, I., Georgiou, D. K. & Vekilov, P. G. (2003). Capillarity effects on the crystallization kinetics: insulin. *J. Am. Chem. Soc.* **125**, 11684–11693.
 33. Kaischew, R. & Stranski, I. N. (1937). Über die Thomson–Gibbs'sche Gleichung bei Kristallen. *Z. Phys. Chem. B*, **35**, 427–432.
 34. McPherson, A., Malkin, A. J. & Kuznetsov, Y. G. (1995). The science of macromolecular crystallization. *Structure*, **3**, 759–768.
 35. McPherson, A., Malkin, A. J. & Kuznetsov, Yu. G. (2000). Atomic force microscopy in the study of macromolecular crystal growth. *Annu. Rev. Biophys. Biomol. Struct.* **29**, 361–410.
 36. Lin, H., Yau, S.-T. & Vekilov, P. G. (2003). Dissipating step bunches during crystallization under transport control. *Phys. Rev. E*, **67**, 0031606.
 37. Kuznetsov, Y. G., Malkin, A. J. & McPherson, A. (1999). AFM studies of the nucleation and growth mechanisms of macromolecular crystals. *J. Crystal Growth*, **196**, 489–502.
 38. Gliko, O., Neumaier, N., Fischer, M., Haase, I., Bacher, A., Weinkauff, S. & Vekilov, P. G. Dense liquid droplets as a step source for the crystallization of lumazine synthase. *J. Crystal Growth*, in press.
 39. Vekilov, P. G. & Alexander, J. I. D. (2000). Dynamics of layer growth in protein crystallization. *Chem. Rev.* **100**, 2061–2089.
 40. Vekilov, P. G. (2003). Molecular mechanisms of defect formation. In *Methods in Enzymology* (Carter, C. W. & Sweet, R. M., eds), vol. 368, pp. 170–188, Academic Press, San Diego part C.
 41. Chernov, A. A. (2003). Protein crystals and their growth. *J. Struct. Biol.* **142**, 3–21.
 42. Binnig, G., Quate, C. F. & Gerber, C. (1986). Atomic force microscope. *Phys. Rev. Letters*, **56**, 930–933.
 43. Shao, Z., Mou, J., Czjckowsky, D. M., Yang, J. & Yuan, J. Y. (1996). Biological atomic force microscopy: what is achieved and what is needed. *Advan. Phys.* **45**, 1–86.
 44. Hansma, H. G. (1999). Varieties of imaging with scanning probe microscopes. *Proc. Natl Acad. Sci. USA*, **96**, 14678–14680.
 45. Engel, A. & Müller, D. J. (2000). Observing single biomolecules at work with the atomic force microscope. *Nature Struct. Biol.* **7**, 715–718.
 46. Yau, S.-T. & Vekilov, P. G. (2000). Quasi-planar nucleus structure in apoferritin crystallisation. *Nature*, **406**, 494–497.
 47. Hörber, J. K. H. & Miles, M. J. (2003). Scanning probe evolution in biology. *Science*, **302**, 1002–1005.
 48. Durbin, S. D., Carson, W. E. & Saros, M. T. (1993). *In situ* studies of protein crystal growth by atomic force microscopy. *J. Phys. D*, **26**, B128–B132.
 49. Yau, S.-T., Thomas, B. R. & Vekilov, P. G. (2000). Molecular mechanisms of crystallization and defect formation. *Phys. Rev. Letters*, **85**, 353–356.
 50. Gliko, O., Reviakine, I. & Vekilov, P. G. (2003). Stable equidistant step trains during crystallization of insulin. *Phys. Rev. Letters* 2003;, 90.
 51. Vekilov, P. G. (2004). Microscopic, mesoscopic, and macroscopic lengthscales in the kinetics of phase transformations with proteins. In *Nanoscale Structure and Assembly at Solid–Fluid Interfaces* (De Yoreo, J. J. & Lui, X. Y., eds), pp. 145–200, Kluwer Press, New York.
 52. Lacapere, J. J., Stokes, D. L. & Chatenay, D. (1992). Atomic force microscopy of 3-dimensional membrane-protein crystals—Ca-ATPase of sarcoplasmic-reticulum. *Biophys. J.* **63**, 303–308.
 53. Malkin, A. J. & McPherson, A. (2004). Probing of crystal interfaces and the structures and dynamic properties of large macromolecular ensembles with *in situ* atomic force microscopy. In *From Fluid–Solid Interfaces to Nanostructural Engineering* (De Yoreo, J. J. & Lui, X. Y., eds), vol. 2, pp. 201–238, Plenum/Kluwer Academic, New York.
 54. Neff, G. A., Gragson, D. E., Shon, D. A. & Baker, S. M.

- (1999). Anomalous lateral size measurements by atomic force microscopy in a fluid cell. *Langmuir*, **15**, 2999–3002.
55. Reviakine, I., Bergsma-Schutter, W. & Brisson, A. (1998). Growth of protein 2-d crystals on supported planar lipid bilayers imaged *in situ* by AFM. *J. Struct. Biol.* **121**, 356–362.
56. Muller, D. J., Schabert, F. A., Buldt, G. & Engel, A. (1995). Imaging purple membranes in aqueous-solutions at subnanometer resolution by atomic-force microscopy. *Biophys. J.* **68**, 1681–1686.
57. Petsev, D. N., Chen, K., Gliko, O. & Vekilov, P. G. (2003). Diffusion-limited kinetics of the solution–solid phase transition of molecular substances. *Proc. Natl Acad. Sci. USA*, **100**, 792–796.
58. Rashkovich, L. N. (1991). *KDP-Family Single Crystals*. Adam Hilger, Bristol, UK.
59. Zaitseva, N. & Carman, L. (2001). Rapid growth of KDP-type crystals. *Prog. Crystal Growth Characterization Mater.* **43**, 1–118.
60. Chernov, A. A. (1999). Estimates of internal stress and related mosaicity in solution grown crystals: proteins. *J. Crystal Growth*, **196**, 524–534.
61. Yau, S.-T., Thomas, B. R., Galkin, O., Gliko, O. & Vekilov, P. G. (2001). Molecular mechanisms of microheterogeneity-induced defect formation in ferritin crystallization. *Proteins: Struct. Funct. Genet.* **43**, 343–352.
62. Van den Hoek, B., Van der Eerden, J. P. & Bennema, P. (1982). Thermodynamic stability conditions for the occurrence of hollow cores caused by stress of line and planar defects. *J. Crystal Growth*, **56**, 621–632.
63. Vekilov, P. G., Alexander, J. I. D. & Rosenberger, F. (1996). Nonlinear response of layer growth dynamics in the mixed kinetics-bulk transport regime. *Phys. Rev. E*, **54**, 6650–6660.
64. Lorber, B. & Delucas, L. J. (1990). Large-scale preparation of homogeneous bacteriorhodopsin. *FEBS Letters*, **261**, 14–18.
65. Nollert, P., Navarro, J. & Landau, E. M. (2002). Crystallization of membrane proteins in cubo. *G Protein Pathways, Pt a, Receptors*, **343**, 183–199.
66. Nollert, P. & Landau, E. M. (1998). Enzymic release of crystals from lipidic cubic phases. *Biochem. Soc. Trans.* **26**, 709–713.
67. Muller, D. J., Amrein, M. & Engel, A. (1997). Adsorption of biological molecules to a solid support for scanning probe microscopy. *J. Struct. Biol.* **119**, 172–188.
68. Vekilov, P. G., Ataka, M. & Katsura, T. (1993). Laser Michelson interferometry investigation of protein crystal growth. *J. Crystal Growth*, **130**, 317–320.
69. Vekilov, P. G., Ataka, M. & Katsura, T. (1995). Growth processes of protein crystals revealed by laser Michelson interferometry investigation. *Acta Crystallog. sect. D*, **51**, 207–219.
70. Hansma, P. K., Cleveland, J. P., Radmacher, M., Walters, D. A., Hillner, P. E., Bezaniilla, M. *et al.* (1994). Tapping mode atomic-force microscopy in liquids. *Appl. Phys. Letters*, **64**, 1738–1740.
71. Schaffer, T. E., Cleveland, J. P., Ohnesorge, F., Walters, D. A. & Hansma, P. K. (1996). Studies of vibrating atomic force microscope cantilevers in liquid. *J. Appl. Phys.* **80**, 3622–3627.

Edited by I. Wilson

(Received 15 June 2004; received in revised form 26 August 2004; accepted 14 September 2004)